

## Article

# A Semi-Octagonal 40-Bit High Capacity Chipless RFID Tag for Future Product Identification

Usman A. Haider<sup>1</sup>, Muhammad Noman<sup>1</sup> , Aamir Rashid<sup>2</sup>, Hatem Rmili<sup>3,4</sup>, Hidayat Ullah<sup>1</sup>   
and Farooq A. Tahir<sup>1,\*</sup>

<sup>1</sup> School of Electrical Engineering and Computer Science, National University of Sciences and Technology, Islamabad 44000, Pakistan

<sup>2</sup> Department of Electronics Engineering, University of Engineering and Technology, Taxila 47050, Pakistan

<sup>3</sup> K.A. CARE Energy Research and Innovation Center, King Abdulaziz University, Jeddah 21589, Saudi Arabia

<sup>4</sup> Electrical and Computer Engineering Department, Faculty of Engineering, King Abdulaziz University, Jeddah 21589, Saudi Arabia

\* Correspondence: farooq.tahir@seecs.edu.pk; Tel.: +92-3336692822

**Abstract:** This paper presents a unique geometry of a chipless radio frequency identification (RFID) tag for encoding a large number of bits in a very small form factor. The tag geometry consists of semi-octagonal copper strips, sequentially laid on a single side of an ultra-thin substrate. A unique and robust encoding mechanism for the tag identification (ID) is proposed. The operating frequency spectrum of the tag ranges from 3.1 to 10.5 GHz. The tag is compact, having an overall size of  $14.5 \times 28 \text{ mm}^2$ . The proposed tag exhibits very high code density of  $9.85 \text{ bits/cm}^2$  and spectral efficiency of  $5.4 \text{ bits/GHz}$ . The unique geometric configuration of the proposed tag allows it to encode up to 40 bits of data as an RCS signature. This chipless RFID tag seems to be a potential candidate for a wide range of modern RFID applications.

**Keywords:** barcode; chipless RFID; frequency domain; future systems miniaturization; product identification; RCS; tag



**Citation:** Haider, U.A.; Noman, M.; Rashid, A.; Rmili, H.; Ullah, H.; Tahir, F.A. A Semi-Octagonal 40-Bit High Capacity Chipless RFID Tag for Future Product Identification. *Electronics* **2023**, *12*, 349. <https://doi.org/10.3390/electronics12020349>

Academic Editors: Reza K. Amineh and Hirokazu Kobayashi

Received: 14 October 2022  
Accepted: 27 November 2022  
Published: 10 January 2023



**Copyright:** © 2023 by the authors. Licensee MDPI, Basel, Switzerland. This article is an open access article distributed under the terms and conditions of the Creative Commons Attribution (CC BY) license (<https://creativecommons.org/licenses/by/4.0/>).

## 1. Introduction

For many years, optical barcode technology has been utilized in many different situations for reading, tracking, identification, and monitoring of objects because of its low cost and reliability [1]. Recent advancements in computing, communications, and automated systems have raised concerns regarding the constraints of the barcode technology. This includes tight human machine interface (HMI), lack of security, line-of-sight (LoS), and the reading range of barcode systems. To overcome these constraints, the radio frequency identification (RFID) technique is now being utilized [2]. An RFID system consists of a transceiver, an electronic tag, and a reader. These new RFID systems offer automated operation, higher security, longer range, and larger data capacities compared to previous barcode systems. They are thus superior in their working and can be applied to scenarios such as vehicle identification, shopping products, employee card readings, and cargo inventory management. It had been estimated that RFID tags would be used by billions of products in future [3].

There are two types of tags employed in RFID systems: (1) with on-board electronics and (2) without any electronics. The latter type, without electronics, is called a chipless RFID tag, as has a significantly reduced cost compared to the chipped tag. Chipless RFID (CRFID) tags are therefore of great importance to the research community. Data encoding methodologies and capacity enhancement of a CRFID tag are ongoing research challenges. Many different encoding techniques have been presented in the literature. Four primary encoding techniques are used [4]: (1) time-domain (TD); (2) frequency-domain (FD); (3) spatial-domain; and (4) hybrid encoding techniques [5–10]. The FD-based CRFID

tags are further divided into (1) backscattering and (2) retransmission-based tags. In the former case, an electromagnetic (EM) wave impinging on the tag is reflected by the tag and its radar cross-section (RCS) is computed. The RCS contains an electromagnetic signature that corresponds to the information stored on that particular tag [11–14]. FD-based CRFID tags are being designed to address different challenges of the market, such as cost, bit capacity, code density, spectral efficiency, compactness, and robustness [15–27].

For this purpose, different state-of-the-art CRFID tags based on the FD technique are reported in the literature. In [18], a closed loop elliptical shaped tag operating from 3.5 to 15.5 GHz with a code density of 2.74 bits/cm<sup>2</sup> and a spectral efficiency of 0.83 bits/GHz is reported. A novel trefoil-shaped tag [19] having an overall size of 13.55 × 13.55 mm<sup>2</sup> and a high code density of 5.44 bits/cm<sup>2</sup>, operating from 5.4 to 10.4 GHz with spectral bit efficiency of 2 bit/GHz, was investigated. Similarly, some closed-loop resonators [20,21] with butterfly- and kite-shaped tags operating in 4.7–10 GHz with a spectral efficiency of 2 bits/GHz, having a high code density of 5.1 and 5.44 bits/cm<sup>2</sup>, respectively, have been presented. All the above discussed closed-loop tags [18–21] bear an overall compact size and high code densities but low spectral efficiency.

Moreover, recently reported open-loop resonating CRFID tags [22–27] are also available. A novel L-shaped design [23] operating within 3–6 GHz with a high code density and spectral efficiency of 4 bits/cm<sup>2</sup> and 5.33 bit/GHz, respectively, has been reported. However, it has a low bit capacity of only 8 bits. A semi-elliptical shaped tag with a slightly higher code density of 4.7 bits/cm<sup>2</sup> was presented in [24]. This tag operates in a wide band of 4.1–16 GHz, exhibiting a very low spectral efficiency of 1.68 bits/GHz. In [25], a capacitive loaded dipole-based tag with a very high spectral efficiency of 12.5 bits/GHz operating at 2–3.6 GHz was proposed. The tag possesses a very large size of 16.7 × 67.8 mm<sup>2</sup>, resulting in a low code density of 1.77 bits/cm<sup>2</sup>. A 21-bit coupled-line micro strip-based tag having a high spectral efficiency of 7 bits/GHz and a very large size of 60.3 × 11 mm<sup>2</sup> with code density of 1.1 bit/cm<sup>2</sup> is discussed in [26]. A very simple rectangular slot-based tag [27] has a spectral efficiency of 1.9 bits/GHz and an overall tag size of 35 × 35 mm<sup>2</sup>. This results in a very low code density of only 0.98 bits/cm<sup>2</sup>. In [28], high-capacity comb-shaped tags are presented. Frequency-domain-based high-capacity tags were recently presented [29] having a closed-loop structure and [30] a 32-bit single quadrant angle-controlled tag. In [31,32], a novel design methodology to design CRFID tags via systematic loading of a square split ring with circular and square slots are presented.

In this work, a unique 40-bit semi-octagon shaped chipless RFID tag is presented. The proposed tag is compact in size, therefore leading to a very high code density. The operating band of the tag is set to between 3.1 and 10.5 GHz, which results in a spectrally efficient design.

## 2. The Tag

### 2.1. Theoretical Design and Coding Scheme

The proposed single layer CRFID tag is designed on a thin Rogers RT Duroid 5880 substrate having a thickness of 0.127 mm. The substrate has permittivity  $\epsilon_r = 2.2$  and loss tangent  $\tan\delta = 0.0009$  mm. The geometrical configuration of the tag is shown in Figure 1 with an overall size ( $L_{\text{sub}} \times W_{\text{sub}}$ ) of 14.5 × 28 mm<sup>2</sup>.

The tag consists of ‘N’ copper strips organized in a nested fashion and separated with gap ‘g’ between them. Each copper strip consists of a pair of two bent segments symmetrically placed around the y-axis. In the right half of the N<sup>th</sup> pair, the first segment has length  $L_{aN}$ , whereas the length of its second segment is  $L_{bN}$ . The bending angles for first and second segments w.r.t. the x-axis are  $\theta_a$  and  $\theta_b$  respectively. The left half of the N<sup>th</sup> copper strip pair is an exact replica of its right half. This particular construction of the proposed tag allows two degrees of freedom in controlling the resonant points of its RCS i.e., by choosing different values for ( $L_{aN}$ ,  $\theta_a$ ) and ( $L_{bN}$ ,  $\theta_b$ ). The back side of the tag has no copper and hence remains empty.

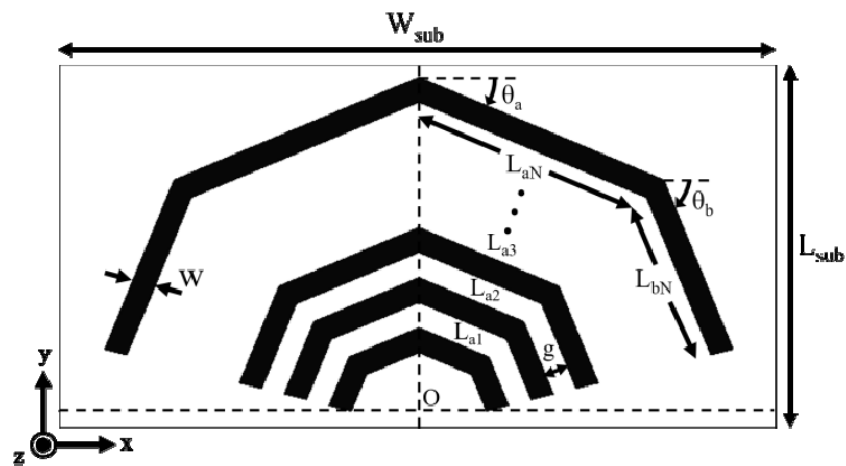


Figure 1. Geometrical configuration of the proposed tag.

The coding scheme used for the proposed tag is frequency-domain based, for which a target band of 3.1–10.5 GHz has been chosen. The spectral allocation for coding of the tag is shown in Figure 2. The RCS operating band is divided into ‘M’ bit-slots, each having 140 MHz of bandwidth. All bit-slots are separated by a guard band of 45 MHz. A bit-slot starts at the frequency ‘ $f_{aM}$ ’ and ends at ‘ $f_{bM}$ ’, such that  $f_{bM} = f_{aM} + 140$  MHz. For the particular bands chosen here, there are  $M = 40$  bit-slots and hence 40 bits can be encoded. The lowest frequency bit-slot i.e., ‘Bit Slot 1’, is designated as the least significant bit of the tag ID. Therefore, the highest frequency bit slot i.e., ‘Bit Slot M’, corresponds to the most significant bit. At this point, it is worth mentioning that the total number of copper strips ‘N’ present on the tag (Figure 1) is not equal to the total number of allocated bit-slots ‘M’ (Figure 2).

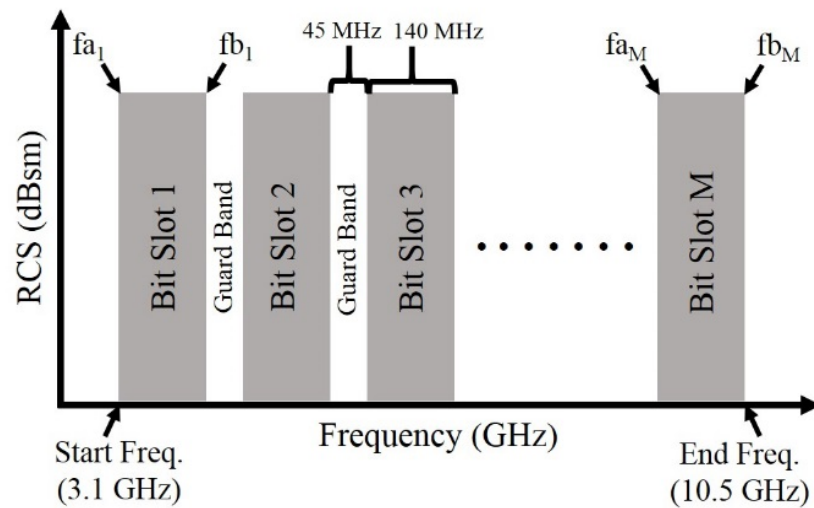


Figure 2. The spectral allocation for the proposed tag.

Furthermore, the RCS magnitude is divided into three regions as shown in Figure 3. The levels of these three regions have been labeled as: (1) valid logic bit 0, (2) invalid logic bit, and (3) valid logic bit 1. The bounding values for these levels are set as 0 to  $-38.5$ ,  $-38.5$  to  $-41.5$ , and  $-41.5$  to  $-\infty$  dBsm. The mechanism to encode a valid bit, therefore, is that the RCS must exist between the bounds specified in Figures 2 and 3. These bounds are summarized in Table 1, for correct decoding of a tag’s ID from its RCS response.

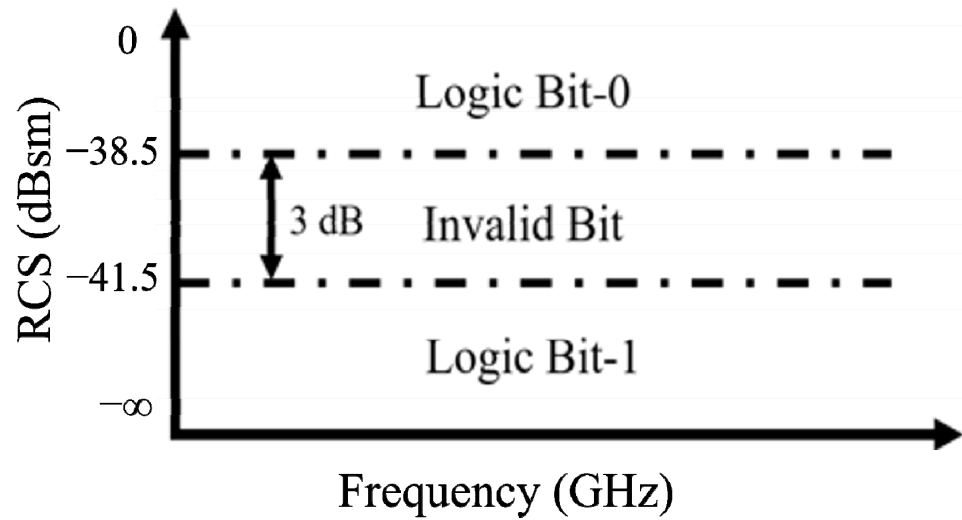


Figure 3. The RCS response allocation.

Table 1. Summary of bit decoding process.

Case	Frequency Range, $f$ (GHz)	RCS Magnitude Range (dBsm)	Decoded Logic
1	$F_{aM} < f < F_{bM}$	$ RCS  > -38.5$	0
2	$F_{aM} < f < F_{bM}$	$ RCS  < -41.5$	1
3	$F_{aM} < f < F_{bN}$	$-38.5 >  RCS  > -41.5$	invalid
4	$F_{aM-1} < f < F_{aM}$	$ RCS  > 0$	invalid

There is a two-step process to encode a logic bit 0 at a particular bit-slot. First, a length corresponding to the central frequency of the bit-slot is roughly calculated using the following standard formulation:

$$L_N = \frac{c}{2f} \sqrt{\frac{2}{\epsilon_r + 1}} \tag{1}$$

where ‘ $c$ ’ is the speed of light, ‘ $f$ ’ is the central frequency of the desired bit slot, and ‘ $\epsilon_r$ ’ is the permittivity of the substrate used. In the second step, lengths  $L_{aN}$  and  $L_{bN}$  are chosen iteratively, such that the following relationship remains true:

$$L_N = 2(L_{aN} + L_{bN}) \tag{2}$$

where  $L_{aN}$  and  $L_{bN}$  are the segment lengths at angles  $\theta_a$  and  $\theta_b$ , respectively. It must be mentioned here that for the proposed tag design, a constant value of  $22.5^\circ$  has been chosen for  $\theta_a$  whereas,  $\theta_b = 2\theta_a$  for all the ‘ $N$ ’ copper strips.

### 2.2. Single Bit Resonator

A single bit resonator (i.e.,  $N = 1$ ) based on the theoretical tag design scheme was simulated to show the effect of  $L_N$  on RCS. This effect is shown as a parametric analysis graph in Figure 4. It can clearly be noticed that by controlling the length  $L_N$ , the peak value of RCS can be varied over a large spectrum. It is also noticed that the RCS response of the single bit resonator has a significant bandwidth and will therefore occupy more than a single bit-slot. This phenomenon will result in lessor number of copper strips ‘ $N$ ’ than ideally required.

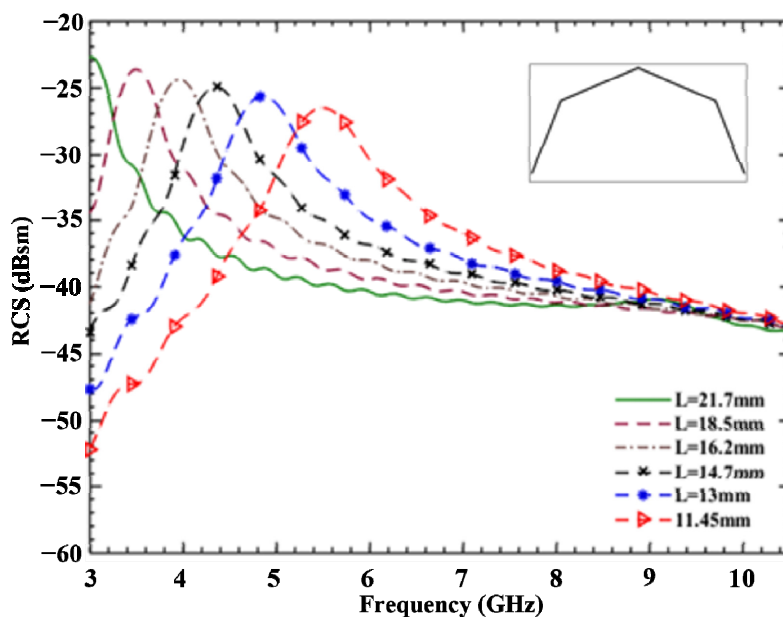


Figure 4. Effect of  $L_N$  for a single bit resonator.

### 2.3. Tag Configurations

Several tag configurations of the above discussed tag were designed and simulated to verify the proposed concept. Four of the configurations, namely, Tag 1, Tag 2, Tag 3, and Tag 4 bearing different 40-bit IDs are outlined in Table 2.

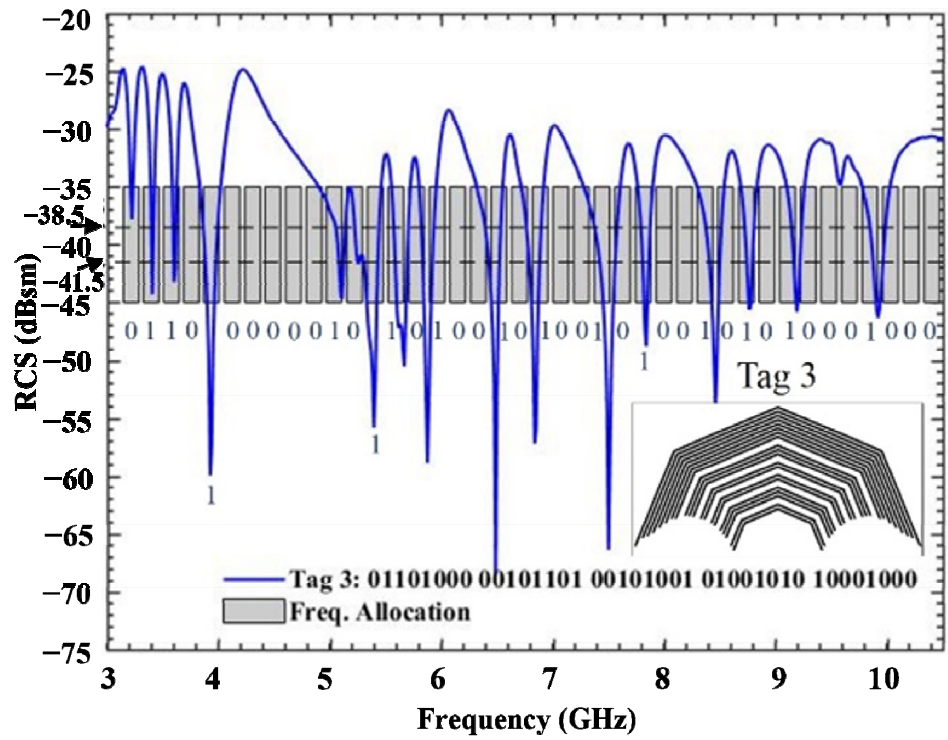
Table 2. List of Tags and their ID's.

S. No	Tag Name	Tag 40-Bit ID
1	Tag 1	01101101 00101101 10101010 11010100 10000100
2	Tag 2	10010010 01000100 10010010 00100010 00001000
3	Tag 3	01101000 00101101 00101001 01001010 10001000
4	Tag 4	10100001 10010100 10100001 00000010 00010100

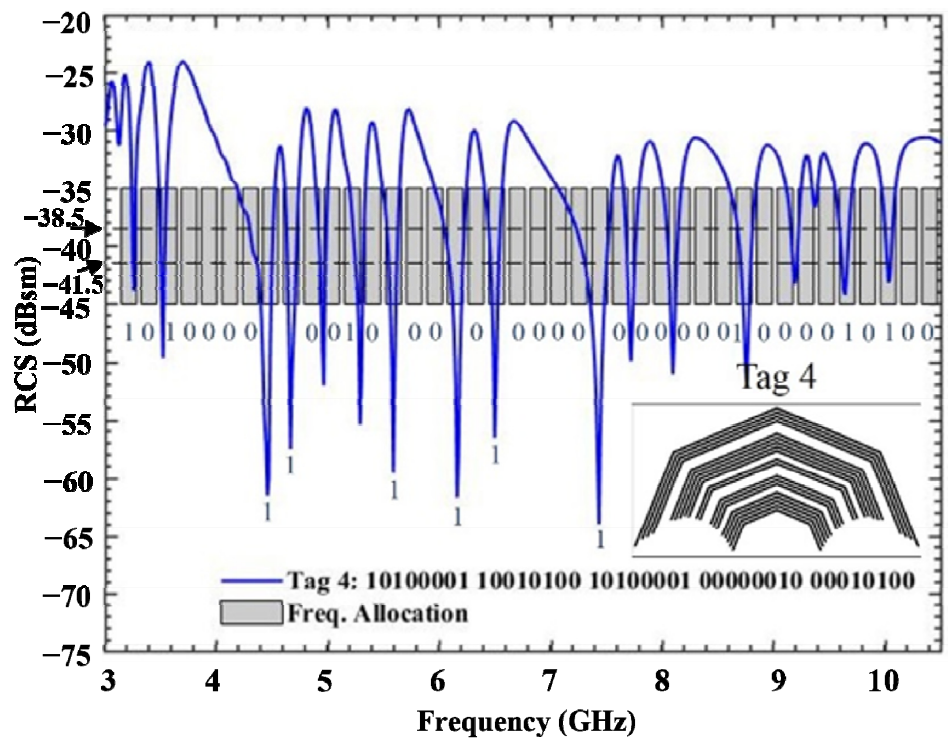
All the above listed tags were designed with the same overall dimension of  $14.5 \times 28 \text{ mm}^2$ . The element width 'w' and the spacing  $g = 0.2 \text{ mm}$  between them was also kept the same. The distance 'd' of first element from point 'o' was kept at 3.2 mm throughout all the designs. The RCS responses of all the tags (Tag 1–4) are shown in Figure 5. The geometries of the resulting tags generated for their respective IDs are shown alongside their RCS graphs.

The RCS thresholds and bit-slot's frequency bands are represented by grey-colored rectangular blocks, as shown in Figure 5. Each tag has a different number of copper strips 'N', to encode a 40-bit ID. For example, Tag 1 has  $N = 25$ , for Tag 2  $N = 13$ , for Tag 3  $N = 20$ , and for Tag 4  $N = 19$ . Using the grey threshold bounds in Figure 5, a tag ID can be found easily. For example, for tag 1, it can be seen that the ID can be decoded by comparing the RCS magnitudes to the threshold levels provided in Table 1. Looking into bit-slot 1, the RCS resonance is in logic bit '0' region (0 to  $-38.5 \text{ dBsm}$ ), so it is encoded as '0'. For bit-slot 2, the RCS resonance crosses the logic bit '1' region, so it is encoded as '1'. For bit-slot 35, the RCS magnitude lies between the invalid region ( $-38.5$  to  $-41.5 \text{ dBsm}$ ) and the transition region, so it is encoded as '0'. All other bit-slots have been encoded in the same manner, and therefore can be decoded accordingly. Alternatively, using the limits provided in Table 1, a tag's ID can be computed through digital signal processing. Optimized parameters of Tag 1 are provided in Table 3. The parameters for the rest of three tags are not shown here for brevity.





(c)



(d)

Figure 5. Simulated RCS responses: (a) Tag 1; (b) Tag 2; (c) Tag 3; (d) Tag 4.

**Table 3.** List of optimized parameters for Tag 1.

Parameter	Value (mm)	Parameter	Value (mm)	Parameter
L <sub>a1</sub>	3.52	L <sub>a18</sub>	8.72	L <sub>b10</sub>
L <sub>a2</sub>	3.82	L <sub>a19</sub>	9.03	L <sub>b11</sub>
L <sub>a3</sub>	4.13	L <sub>a20</sub>	9.33	L <sub>b12</sub>
L <sub>a4</sub>	4.43	L <sub>a21</sub>	9.64	L <sub>b13</sub>
L <sub>a5</sub>	4.74	L <sub>a22</sub>	9.94	L <sub>b14</sub>
L <sub>a6</sub>	5.05	L <sub>a23</sub>	10.25	L <sub>b15</sub>
L <sub>a7</sub>	5.35	L <sub>a24</sub>	10.56	L <sub>b16</sub>
L <sub>a8</sub>	5.66	L <sub>a25</sub>	10.87	L <sub>b17</sub>
L <sub>a9</sub>	5.97	L <sub>b1</sub>	2.87	L <sub>a18</sub>
L <sub>a10</sub>	6.27	L <sub>b2</sub>	2.74	L <sub>b19</sub>
L <sub>a11</sub>	6.68	L <sub>b3</sub>	2.61	L <sub>b20</sub>
L <sub>a12</sub>	6.89	L <sub>b4</sub>	2.49	L <sub>b21</sub>
L <sub>a13</sub>	7.19	L <sub>b5</sub>	2.51	L <sub>b22</sub>
L <sub>a14</sub>	7.5	L <sub>b6</sub>	2.45	L <sub>b23</sub>
L <sub>a14</sub>	7.5	L <sub>b6</sub>	2.45	L <sub>b23</sub>
L <sub>a15</sub>	7.8	L <sub>b7</sub>	2.43	L <sub>b24</sub>
L <sub>a16</sub>	8.11	L <sub>b8</sub>	2.52	L <sub>b25</sub>
L <sub>a17</sub>	8.41	L <sub>b9</sub>	2.5	-

The least significant bit for Tag 1 exists at 3.2 GHz, while its most significant bit occurs at 10.1 GHz. The code density of the proposed tag is calculated to be 9.85 bits/cm<sup>2</sup> and its spectral efficiency is 5.4 bits/GHz. These values are much higher than those of various recently published state-of-the-art CRFID tags. The comparison in Table 4 shows that the proposed tag exhibits better performance when considering code density and spectral efficiency.

**Table 4.** Comparison with state-of-the-art CRFID tags.

Ref. No.	Tag Structure	Operating Frequency (GHz)	Size (mm <sup>2</sup> )	No. of Bits	Code Density (Bits/cm <sup>2</sup> )	Spectral Efficiency (Bits/GHz)
[18]	Elliptical Slot	3.5–15.5	22.8 × 16	10	2.74	0.83
[19]	Trefoil-Shaped Slot	5.4–10.4	13.55 × 13.55	10	5.44	2
[20]	Butterfly Slot	4.7–9.7	14 × 14	10	5.1	2
[21]	kite-shaped resonators	4.7–10	13.55 × 13.55	10	5.44	2
[22]	Circularly Arranged Scatters	1.8–3.6	55 × 55	20	0.7	12.5
[23]	L-Shaped Slots	3–6	20 × 20	8	4	5.33
[24]	Semi-Elliptical Shaped Slots	4.1–16	25 × 17	20	4.70	1.68
[25]	Spiral C-loaded Scatters	2–3.6	16.7 × 67.8	20	1.77	12.5
[26]	Coupled Line Micro Strip Resonator	5–8	60.3 × 11	21	1.1	7
[27]	Rectangular Slot Ring	2–9	35 × 35	12	0.98	1.9
Proposed Tag	Semi-Regular Octagon Shaped Strips	3.1–10.5	14.5 × 28	40	9.85	5.40

The surface current distribution of the proposed tag (Tag 1) at four different frequencies when the y-polarized plane wave is incident upon them is shown in Figure 6a–d. It can clearly be observed that the outer copper strips are sensitive to lower frequencies, whereas the inner copper strips become active at higher frequencies. It can also be observed that

there exists mutual coupling between the nearby tag strips, which is believed to result in a wider RCS response. This mutual coupling effect can be minimized by increasing the separation between the strips.

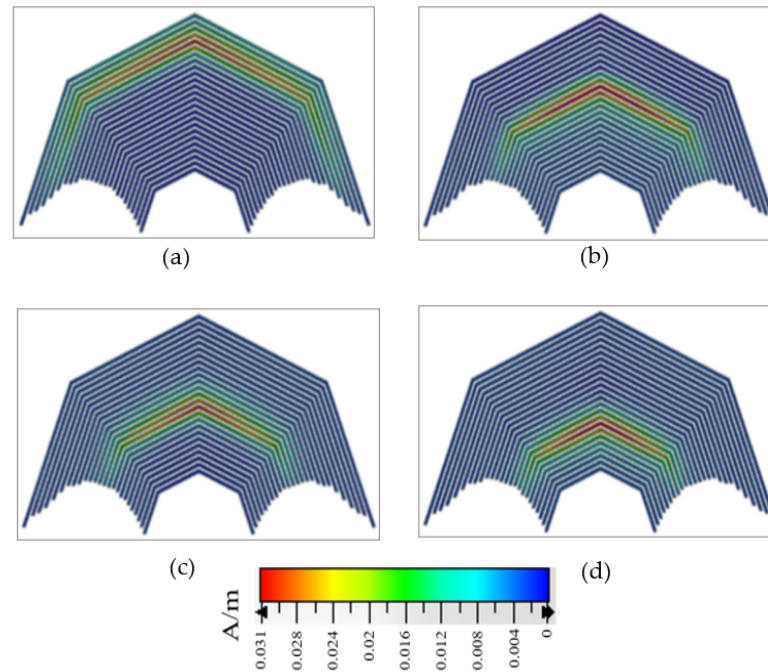


**Figure 6.** Surface current distribution at: (a) 4 GHz; (b) 6 GHz; (c) 7 GHz; (d) 8 GHz.

### 3. Fabrication and Measurement Results

To verify the RCS response, all four tags were fabricated as shown in Figure 7. The fabrication was carried out by a standard PCB process on a thin 0.127 mm Rogers 5880 substrate. The fabricated tags were measured through a vector network analyzer (VNA) in an anechoic chamber. The photograph of the measurement setup is shown in Figure 8.

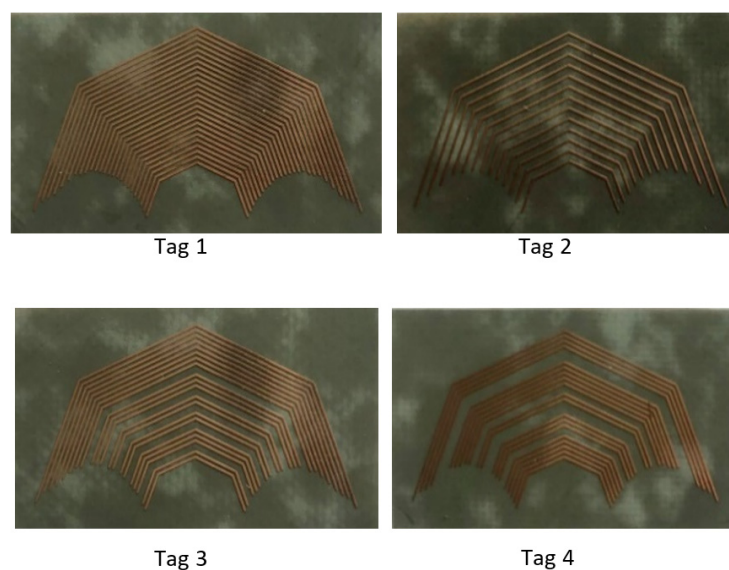


**Figure 7.** Fabricated prototypes of the tags.

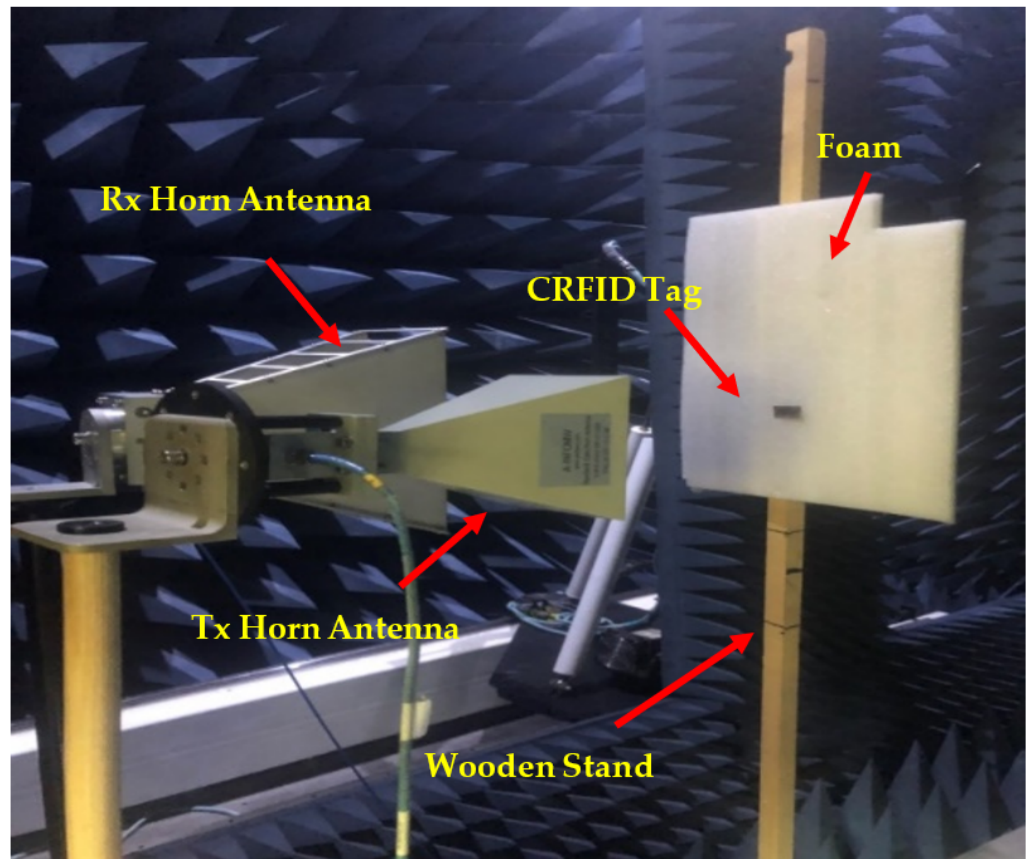


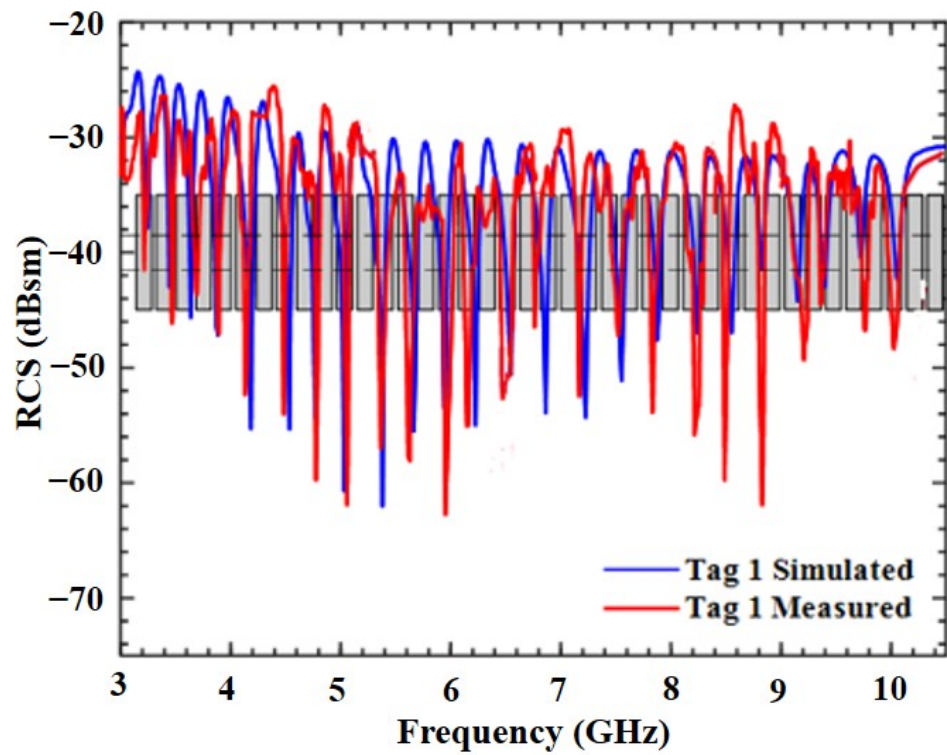
**Figure 8.** Measurement setup: Panoramic photograph inside an anechoic chamber.

The fabricated tag was placed at far-field distance from the feed horns and S parameter  $S_{21}$  was measured. To filter out the static noise from the measured results, the reference measurements without the tag were also made. To plot the RCS of all the fabricated tags, the following mathematical expression [33] was used:

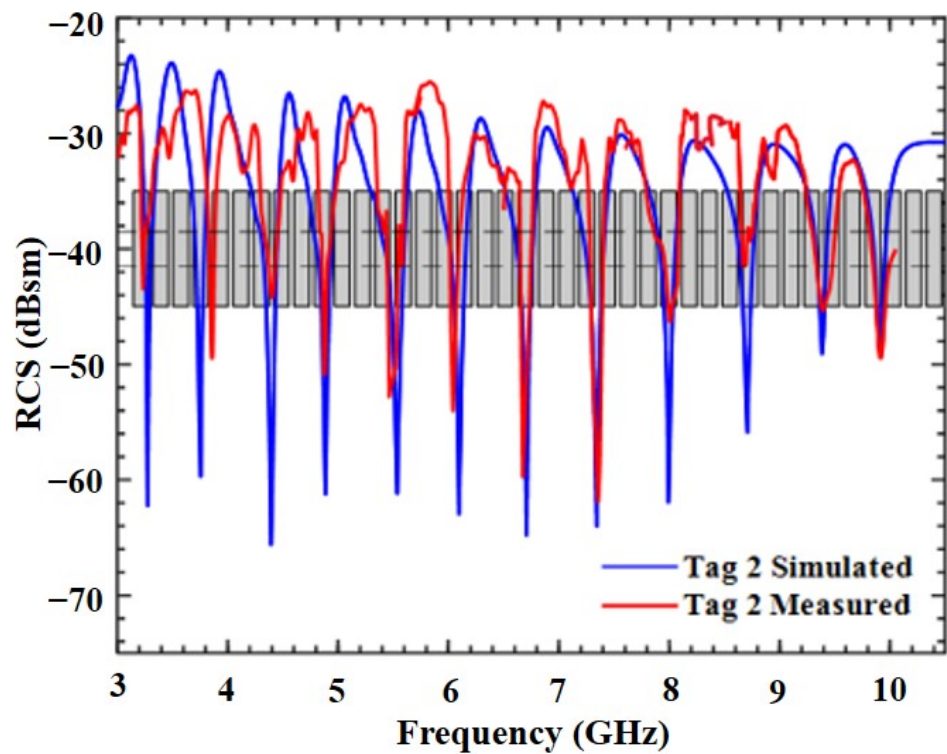
$$\delta^{tag} = \left[ \frac{s_{21}^{tag} - s_{21}^{isolation}}{s_{21}^{ref} - s_{21}^{isolation}} \right]^2 \cdot \delta^{ref} \quad (3)$$

where  $\delta^{ref}$  is a predetermined RCS response of a rectangular metal plate,  $s_{21}^{isolation}$  is the transmission response of the anechoic chamber setup without the tag,  $s_{21}^{ref}$  is the transmission coefficient of a large metal sheet, and  $s_{21}^{tag}$  is the transmission coefficient in presence of the tag. The RCS measurement was performed using three different standard gain horn antennas (SGHA): (1) 2–3.95 GHz; (2) 3.95–5.85 GHz; and (3) 5.85–8.20 GHz as transmitters.

The reception was achieved via a wide band horn antenna operating at 2–18 GHz. The tags were attached to foam. To filter out the effects of the foam and the surroundings, a separate measurement was taken without the tag, and only with the foam. The  $S_{21}$  of this measurement was then subtracted from the tag response. The measured and simulated RCS responses of Tags 1–4 are shown in Figure 9. The measured results are in good correlation with those simulated.

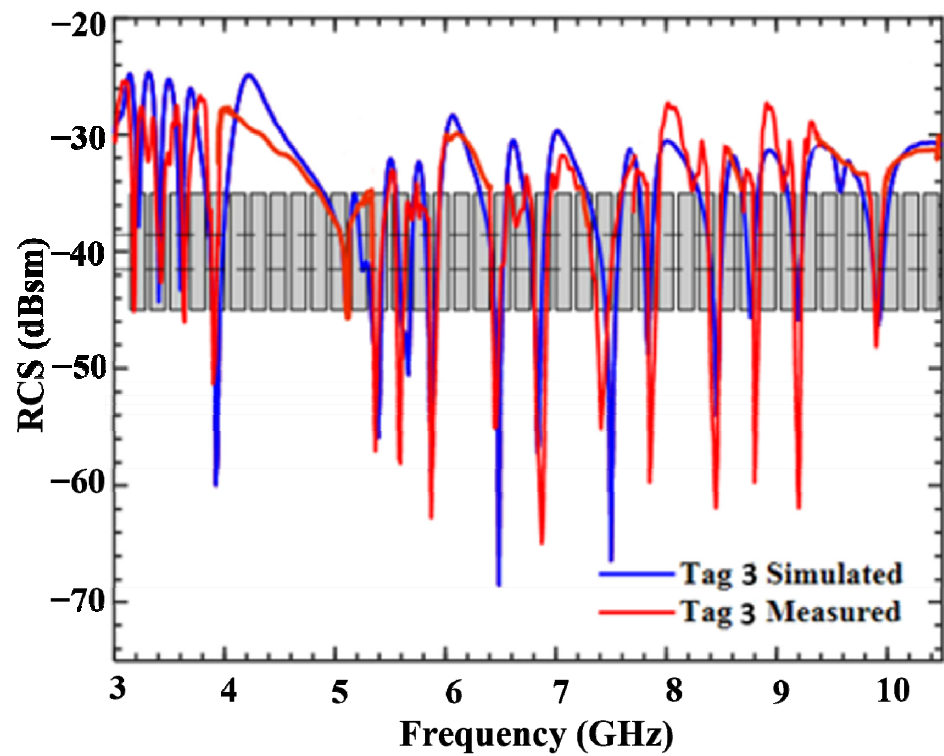


(a)

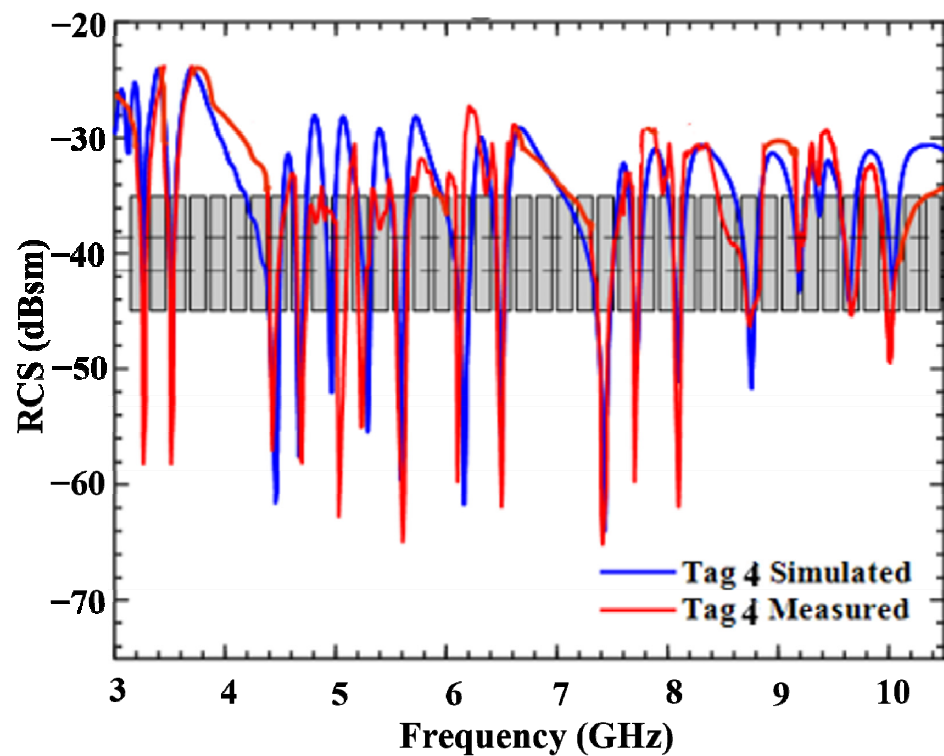


(b)

Figure 9. Cont.



(c)



(d)

Figure 9. The measured RCS responses of CRFID tag: (a) Tag 1; (b) Tag 2; (c) Tag 3; (d) Tag 4.

#### 4. Conclusions

A unique geometrical configuration for a chipless RFID tag was presented. The proposed tag was modeled on an ultra-thin Rogers substrate. The tag is extremely compact,

bearing a footprint of  $14.5 \times 28 \text{ mm}^2$  and having a very high code density of  $9.85 \text{ bit/cm}^2$ . The operating frequency range of the tag is from 3.1 to 10.5 GHz. The tag was found to be spectrally very efficient with efficiency equal to  $5.4 \text{ bits/GHz}$ . The proposed tag could easily store up to 40 bits, even with a lesser amount of on-board copper resonators. This specially designed compact and ultra-thin chipless RFID tag can be used by RFID system designers for various identification applications.

**Author Contributions:** U.A.H., M.N., A.R., and H.U. designed, simulated, and fabricated the prototypes. They also performed the measurements and wrote the manuscript. F.A.T. conceived the idea, supervised the whole work, and revised the draft. H.R. contributed to the concept, analyzed the results, and interpreted the data. All authors have read and agreed to the published version of the manuscript.

**Funding:** This project was funded by King Abdullah City for Atomic and Renewable Energy (K.A. CARE) under K.A. CARE-King Abdulaziz University Collaboration Program, and the Deanship of Scientific Research, King Abdulaziz University vide grant number (RG-14-135-43).

**Data Availability Statement:** Not applicable.

**Acknowledgments:** The authors acknowledge the support provided by King Abdullah City for Atomic and Renewable Energy (K.A. CARE) under K.A. CARE-King Abdulaziz University Collaboration Program. The authors are also thankful to Deanship of Scientific Research, King Abdulaziz University for providing financial vide grant number (RG-14-135-43).

**Conflicts of Interest:** The authors declare no conflict of interest.

## References

1. Preradovic, S.; Karmakar, N.C. Chipless RFID: Bar code of the future. *IEEE Microw. Mag.* **2010**, *11*, 87–97. [[CrossRef](#)]
2. Rezaiesarlak, R.; Manteghi, M. *Chipless RFID: Design Procedure and Detection Techniques*; Springer: Berlin/Heidelberg, Germany, 2016.
3. Khan, M.M.; Tahir, F.A.; Cheema, H.M. Frequency Band Utilization Enhancement for Chipless RFID Tag through Place Value Encoding. In Proceedings of the IEEE International Antennas and Propagation Symposium and USNC-URSI Radio Science Meeting, Fajardo, PR, USA, 26 June–1 July 2016; pp. 1477–1478.
4. Pöpperl, M.; Parr, A.; Mandel, C.; Jakoby, R.; Vossiek, M. Potential and practical limits of time-domain reflectometry chipless RFID. *IEEE Trans. Microw. Theory Tech.* **2016**, *64*, 2968–2976. [[CrossRef](#)]
5. Kalansuriya, P.; Karmakar, N.C.; Viterbo, E. On the detection of frequency-spectra-based chipless RFID using UWB impulsive interrogation. *IEEE Trans. Microw. Theory Tech.* **2012**, *60*, 4187–4197. [[CrossRef](#)]
6. Khan, M.M.; Tahir, F.A.; Farooqui, M.F.; Shamim, A.; Cheema, H.M. 3.56-bits/cm<sup>2</sup> Compact Inkjet Printed and Application Specific Chipless RFID Tag. *IEEE Antennas Wirel. Propag. Lett.* **2016**, *15*, 1109–1112. [[CrossRef](#)]
7. Feng, C.; Zhang, W.; Li, L.; Han, L.; Chen, X.; Ma, R. Angle-based chipless RFID tag with high capacity and insensitivity to polarization. *IEEE Trans. Antennas Propag.* **2015**, *63*, 1789–1797. [[CrossRef](#)]
8. Jabeen, S.; Ullah, H.; Tahir, F.A. A 26 Bit Alternating U-shaped Chipless RFID Tag Using Slot Length Variation Technique. In Proceedings of the IEEE International Conference on Microwave, Antennas & Circuits (ICMAC), Islamabad, Pakistan, 21–22 December 2021; pp. 1–3.
9. Khan, M.M.; Tahir, F.A.; Cheema, H.M. High Capacity Polarization Sensitive Chipless RFID Tag. In Proceedings of the IEEE International Antennas and Propagation Symposium and USNC-URSI Radio Science Meeting, Vancouver, BC, Canada, 19–24 July 2015; pp. 1770–1771.
10. Islam, M.A.; Karmakar, N.C. Compact Printable Chipless RFID Systems. *IEEE Trans. Microw. Theory Tech.* **2015**, *63*, 3785–3793. [[CrossRef](#)]
11. Zafar, S.; Rubab, S.; Ullah, H.; Tahir, F.A. A 12-bit Hexagonal Chip-less Tag for Radio Frequency Identification Applications. In Proceedings of the 2020 IEEE International Symposium on Antennas and Propagation and North American Radio Science Meeting, Montreal, QC, Canada, 5–10 July 2020; pp. 1503–1504.
12. Salemi, F.; Hassani, H.R.; Mohammad-Ali-Nezhad, S. Linearly Polarized Compact Extended U-shaped Chipless RFID Tag. *AEU-Int. J. Electron. Commun.* **2020**, *117*, 153129. [[CrossRef](#)]
13. Wang, L.; Liu, T.; Sidénn, J.; Wang, G. Design of chipless RFID tag by using miniaturized open-loop resonators. *IEEE Trans. Antennas Propag.* **2018**, *66*, 618–626. [[CrossRef](#)]
14. Islam, M.A.; Karmakar, N.C. A novel compact printable dualpolarized chipless RFID system. *IEEE Trans. Microw. Theory Tech.* **2012**, *60*, 2142–2151. [[CrossRef](#)]
15. Betancourt, D.; Haase, K.; Hübler, A.; Ellinger, F. Bending and folding effect study of flexible fully printed and late-stage coded octagonal chipless RFID tags. *IEEE Trans. Antennas Propag.* **2016**, *64*, 2815–2823. [[CrossRef](#)]

16. Haider, U.A.; Noman, M.; Ullah, H.; Tahir, F.A. A Compact L-Shaped 16 Bit Polarization Independent Chipless RFID Tag. In Proceedings of the 2020 International Conference on UK-China Emerging Technologies (UCET), Glasgow, UK, 20–21 August 2020; pp. 1–3.
17. Haider, U.A.; Noman, M.; Ullah, H.; Tahir, F.A. A Compact Chip-less RFID Tag for IoT Applications. In Proceedings of the 2020 IEEE International Symposium on Antennas and Propagation and North American Radio Science Meeting, Montreal, QC, Canada, 5–10 July 2020; pp. 1449–1450.
18. Jabeen, I.; Ejaz, A.; Riaz, M.A.; Khan, M.J.; Akram, A.; Amin, Y.; Tenhunen, H. Miniaturized Elliptical Slot Based Chipless RFID Tag for Moisture Sensing. *Appl. Comput. Electromagn. Soc. J.* **2019**, *34*, 1366–1372.
19. Tariq, N.; Riaz, M.; Shahid, H.; Khan, M.; Khan, M.; Amin, Y.; Loo, J.; Tenhunen, H. Orientation Independent Chipless RFID Tag Using Novel Trefoil Resonators. *IEEE Access* **2019**, *7*, 122398–122407. [[CrossRef](#)]
20. Riaz, M.; Abdullah, Y.; Shahid, H.; Amin, Y.; Akram, A.; Tenhunen, H. Novel butterfly slot based chipless RFID tag. *Radioengineering* **2018**, *27*, 776–783. [[CrossRef](#)]
21. Tariq, N.; Riaz, M.; Shahid, H.; Khan, M.; Tenhunen, H. A Novel Kite-Shaped Chipless RFID Tag for Low-Profile Applications. *IETE J. Res.* **2019**, *68*, 2149–2156. [[CrossRef](#)]
22. Svanda, M.; Havlicek, J.; Machac, J.; Polivka, M. Polarisation independent chipless RFID tag based on circular arrangement of dual-spiral capacitively-loaded dipoles with robust RCS response. *IET Microw. Antennas Propag.* **2018**, *12*, 2167–2171. [[CrossRef](#)]
23. Sharma, V.; Malhotra, S.; Hashmi, M. Slot Resonator Based Novel Orientation Independent Chipless RFID Tag Configurations. *IEEE Sens. J.* **2019**, *19*, 5153–5160. [[CrossRef](#)]
24. Jabeen, I.; Ejaz, A.; Rahman, M.; Naghshvarianjahromi, M.; Khan, M.; Amin, Y.; Tenhunen, H. Data-Dense and Miniature Chipless Moisture Sensor RFID Tag for Internet of Things. *Electronics* **2019**, *8*, 1182. [[CrossRef](#)]
25. Havlicek, J.; Švanda, M.; Polivka, M.; Machac, J.; Kracek, J. Chipless RFID Tag Based on Electrically Small Spiral Capacitively Loaded Dipole. *IEEE Antennas Wirel. Propag. Lett.* **2017**, *16*, 3051–3054. [[CrossRef](#)]
26. Abdulkawi, W.M.; Sheta, A.-F.A. Four-State Coupled Line Resonator for Chipless RFID Tags Application. *Electronics* **2019**, *8*, 581. [[CrossRef](#)]
27. Ma, Z.; Jiang, Y. High-Density 3D Printable Chipless RFID Tag with Structure of Passive Slot Rings. *Sensors* **2019**, *19*, 2535. [[CrossRef](#)]
28. Babaeian, F.; Karmakar, N. Compact Multi-Band Chipless RFID Resonators for Identification and Authentication Applications. *Electron. Lett.* **2020**, *56*, 724–727. [[CrossRef](#)]
29. Noman, M.; Haider, U.A.; Ullah, H.; Tahir, F.A.; Khan, M.U.; Abbasi, Q.H. 12-Bit Chip-less RFID Tag with High Coding Capacity per Unit Area. In Proceedings of the 2022 IEEE International Symposium on Antennas and Propagation and USNC-URSI Radio Science Meeting (AP-S/URSI), Denver, CO, USA, 10–15 July 2022; pp. 127–128.
30. Noman, M.; Haider, U.A.; Ullah, H.; Tahir, F.A.; Rmili, H.; Najam, A.I. A 32-Bit Single Quadrant Angle-Controlled Chipless Tag for Radio Frequency Applications. *Sensors* **2022**, *22*, 2492. [[CrossRef](#)] [[PubMed](#)]
31. Noman, M.; Haider, U.A.; Ullah, H.; Hashmi, A.M.; Tahir, F.A. Realization of Chipless RFID Tags via Systematic Loading of Square Split Ring with Circular Slots. *IEEE J. Radio Freq. Identif.* **2022**, *6*, 671–679. [[CrossRef](#)]
32. Noman, M.; Haider, U.A.; Hashmi, A.M.; Ullah, H.; Najam, A.I.; Tahir, F.A. A Novel Design Methodology to Realize a Single Byte by Loading a Square Open-Loop Resonator with Micro-Metallic cells. *IEEE J. Microwaves.* **2022**, *12*, accepted. [[CrossRef](#)]
33. Vena, A.; Perret, E.; Tedjini, S. Chipless RFID Tag Using Hybrid Coding Technique. *IEEE Trans. Microw. Theory Tech.* **2011**, *59*, 3356–3364. [[CrossRef](#)]

**Disclaimer/Publisher’s Note:** The statements, opinions and data contained in all publications are solely those of the individual author(s) and contributor(s) and not of MDPI and/or the editor(s). MDPI and/or the editor(s) disclaim responsibility for any injury to people or property resulting from any ideas, methods, instructions or products referred to in the content.